

## Mixing Mechanism of Pulsed Jets with Applications to Fuel Delivery in Combustion Applications

J. Anders<sup>1,2</sup>, M. Ameen<sup>1</sup>, V. Magi<sup>1,3</sup>, and J. Abraham<sup>1,4</sup>

<sup>1</sup>School of Mechanical Engineering  
 Purdue University, West Lafayette, Indiana 47907-2088, USA

<sup>2</sup>Caterpillar, Inc., Peoria, Illinois, USA (current affiliation)

<sup>3</sup>Department of Environmental Engineering and Physics  
 University of Basilicata, 85100 Potenza, Italy

<sup>4</sup>School of Mechanical Engineering  
 University of Adelaide, Adelaide, South Australia 5005, Australia

### Abstract

It has been widely reported that split injection in engines can increase fuel/air mixing and reduce the formation of unburned products of combustion. Large-eddy simulations (LES) of pulsed jets are carried out to understand the mechanism of mixing. The results indicate that in a double injection event, i.e., an injection event with two pulses, an earlier transition and breakup of the head-vortex region in the second pulse occurs as a result of the residual turbulence from the first pulse and reduced rotational strength of the head vortex. The simulations also predict that there is potentially a balance between the effects of the residual bulk velocity to accelerate the second pulse and the effects of the earlier breakup of the head-vortex region to reduce penetration in the second pulse. Depending on the dwell time between the pulses, one or the other of these effects may be dominant. The computed results show faster spreading and slower penetration of the second pulse, relative to the first pulse, once the head vortex interacts with the turbulent eddies remaining from the first injection. The results are related to observed split injection behavior in engines.

### Introduction

Increasing the fuel/air mixing in combustion engines can enhance their combustion efficiency and reduce emissions of toxic pollutants generated as a result of incomplete combustion. In this regard, it has been suggested that pulsed injection, or multiple injection events, can increase fuel/air mixing [15,16]. Jet pulsation has also benefits in enhancing heat transfer, controlling flow separation, and active control of combustion instabilities. In this regard, prior work has shown that jets with sudden decrease in velocity will have an increase in entrainment (mixing) because of a rapid increase in radial influx of ambient fluid [7,8,9,13]. In fact, deceleration and acceleration in unsteady jets can be varied to effect mixing. There is, however, contradictory evidence [20]. In this work, large-eddy simulations (LES) of two-pulse gas jets are carried out and compared with the behaviour of gas jets resulting from a single-injection event to understand the fundamentals of mixing. The justification for using gas jets, as opposed to sprays, is given in Refs. [1, 2] where it is shown that under high-pressure high-temperature conditions encountered in engines, high pressure fuel injection results in fast vaporizing, momentum-controlled jets which can be well-represented by vapour jets.

### The Computational Method

The numerical code employed in this work is FLEDS (Flow-Large Eddy- Direct Simulation) which has been developed in-house primarily for chemically reacting flows [3,4]. The constant-coefficient Smagorinsky model from Erlebacher et al. [12], including the correction to account for compressibility effects, is used. Spatial discretization of the governing equations is performed using a sixth-order accurate non-dissipative compact scheme proposed by Lele [17]. Explicit spatial filtering is performed at every time step to remove subgrid-scale energy and fluctuations, and to maintain numerical stability, using a sixth-order filter proposed by Lele [17]. More detail on the numerics can be found in Refs. [4,17]. Transition to turbulence in the jet is triggered using a vortex-ring perturbation near the inlet in the jet shear layer following Bogey et al. [6]. Boundary conditions follow the method reported by Poinso and Lele [18] in which the relations based on characteristic lines are constructed and then applied to the Navier-Stokes equations. In this work, such an approach has been extended to take into account also the effect of multicomponent gas mixture flows. A compact-storage fourth-order four-stage Runge-Kutta method is used for time integration. The method uses the Gill constants [14] in a formulation found in Carnahan [10].

The Favre-filtered conservation equations for mass, momentum, energy, and species are

$$\frac{\partial \bar{\rho}}{\partial t} + \frac{\partial}{\partial x_j} (\bar{\rho} \tilde{u}_j) = 0, \quad (1)$$

$$\frac{\partial}{\partial t} (\bar{\rho} \tilde{u}_i) + \frac{\partial}{\partial x_j} (\bar{\rho} \tilde{u}_i \tilde{u}_j) = -\frac{\partial \bar{p}}{\partial x_i} + \frac{\partial \tilde{\tau}_{ij}}{\partial x_j}, \quad (2)$$

$$\frac{\partial}{\partial t} (\bar{\rho} \tilde{E}) + \frac{\partial}{\partial x_j} [(\bar{\rho} \tilde{E} + \bar{p}) \tilde{u}_j] = \frac{\partial}{\partial x_j} (\tilde{\tau}_{ij} \tilde{u}_j) \quad (3)$$

$$+ \frac{\partial}{\partial x_j} \left( \tilde{\lambda}_{eff} \frac{\partial \tilde{T}}{\partial x_j} \right) + \frac{\partial}{\partial x_j} \left[ \rho \sum_k \left( \tilde{h}_k \tilde{D}_{eff} \frac{\partial \tilde{Y}_k}{\partial x_j} \right) \right],$$

$$\frac{\partial}{\partial t} (\bar{\rho} \tilde{Y}_k) + \frac{\partial}{\partial x_j} (\bar{\rho} \tilde{Y}_k \tilde{u}_j) = \frac{\partial}{\partial x_j} \left( \bar{\rho} \tilde{D}_{eff} \frac{\partial \tilde{Y}_k}{\partial x_j} \right). \quad (4)$$

The stress tensor in Eq. (2), which is the sum of the resolved and subgrid-scale stress tensors, can be written as

$$\tilde{\tau}_{ij} = \tilde{\mu}_{eff} \left[ \left( \frac{\partial \tilde{u}_i}{\partial x_j} + \frac{\partial \tilde{u}_j}{\partial x_i} \right) - \frac{2}{3} \frac{\partial \tilde{u}_k}{\partial x_k} \delta_{ij} \right] + \frac{1}{3} \tilde{\tau}_{kk} \delta_{ij}. \quad (5)$$

The effective viscosity, conductivity, and diffusivity are defined as the sum of the resolved physical properties and the subgrid-scale modeled turbulent properties. The subgrid-scale turbulent viscosity  $\tilde{\mu}_r$  is modeled using the Smagorinsky subgrid-scale stress model given by

$$\tilde{\mu}_r = C \bar{\rho} \Delta^2 |\tilde{S}|, \quad (6)$$

where  $C$  is a model constant,  $\Delta$  is the filter (often associated with the cell-size) and

$$|\tilde{S}| = \left( 2 \tilde{S}_{ij} \tilde{S}_{ij} \right)^{1/2}. \quad (7)$$

with

$$\tilde{S}_{ij} = \frac{1}{2} \left( \frac{\partial \tilde{u}_i}{\partial x_j} + \frac{\partial \tilde{u}_j}{\partial x_i} \right) \quad (8)$$

The subgrid-scale conductivity is calculated using a turbulent Prandtl number  $Pr_r$  and the specific heat  $C_p$  as

$$\tilde{\lambda}_r = \frac{\tilde{\mu}_r C_p}{Pr_r}. \quad (9)$$

The subgrid-scale diffusivity  $\tilde{D}_r$  is calculated using a specified turbulent Schmidt  $Sc_r$  number as

$$\tilde{D}_r = \frac{\tilde{\mu}_r}{\bar{\rho} Sc_r}. \quad (10)$$

The formulation for the constant-coefficient Smagorinsky model with compressibility comes from Erlebacher et al. [12] The effective stress tensor in Eq. (5) with the subgrid-scale compressibility model is

$$\tilde{\tau}_{ij} = \tilde{\mu}_{eff} \left[ 2 \tilde{S}_{ij} - \frac{2}{3} \tilde{S}_{kk} \delta_{ij} \right] - \frac{2}{3} C_1 \bar{\rho} \Delta^2 |\tilde{S}|^2 \delta_{ij}, \quad (11)$$

where  $C_1$  is a model constant. In the constant-coefficient Smagorinsky model the model coefficients  $C$  and  $C_1$ , along with the turbulent Prandtl and Schmidt numbers, are specified. This allows the subgrid-scale turbulent viscosity, conductivity, and diffusivity to be calculated based on filtered quantities and closes the system of equations. The physical space is discretized using a non-uniform Cartesian grid that can be stretched in all three directions. The non-uniform grid is transformed into a cubed uniformly-spaced grid in the computational space. The resulting tridiagonal systems are solved using the Thomas algorithm [19].

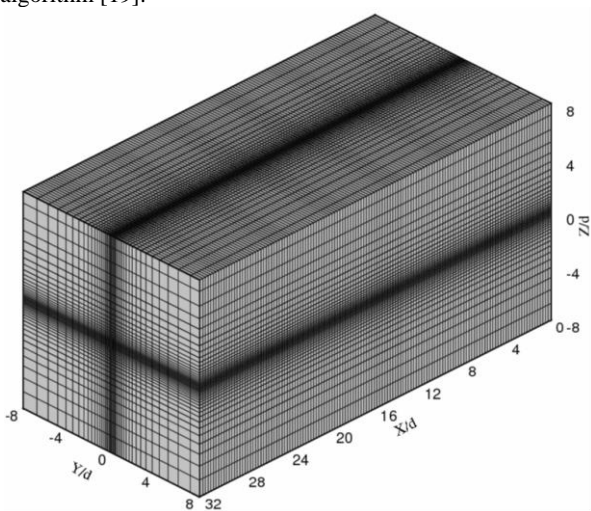
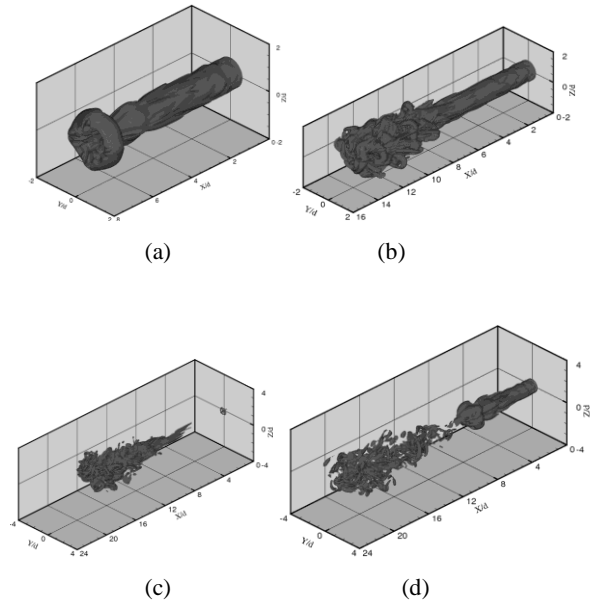


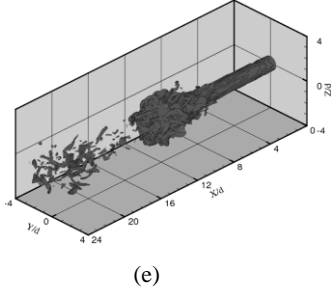
Figure 1. Computational domain (shows every third grid point).

The computational grid/domain employed is shown in Fig. 1. The focus was on the near-field of the jet. The domain extends eight jet diameters in the Y and Z directions and thirty-two diameters in the X (axial) direction. Grid stretching was employed in the Y and Z directions and uniform resolution was used in the axial direction. The resolution was 0.08 jet diameter in X direction and varied from 0.026 to 0.44 in the other two directions. The injection boundary has a sub-sonic inflow condition and all other boundaries were implemented as sub-sonic non-reflecting boundary conditions. The injection velocity is 50 m/s and a co-flow velocity of 0.5 m/s was employed in the rest of the inlet boundary. The injection velocity corresponded to a Reynolds number of 80,000. The maximum Mach number in the domain is 0.1. Other details of the simulations may be found in Ref. [5].

## Results and Discussion

Figure 2 shows a sequence of images of the vorticity iso-surface from a two-pulse injection event showing the interaction of the two pulses. Both pulses have a duration of 0.5 ms separated by a 0.25 ms dwell period. Note that a prior pulse can influence the subsequent pulse through bulk-velocity modification and turbulence modification. In a bulk-sense, this modifies the entrainment. One potential effect of the bulk velocity from a prior injection on a subsequent injection could be to enhance penetration because the velocity field generated by the earlier pulse presents less resistance to jet penetration than the static fluid encountered by an isolated injection. Additionally, the head vortex ring may have less rotational strength because of reduced resistance to penetration faced by an injection into a region of bulk fluid motion established by an earlier injection. This reduced rotational strength of the head vortex ring could lead to an earlier breakup of the coherent structures at the leading edge of the jet. Potential effects of turbulence generated by the first injection include enhancing turbulent mixing of the subsequent pulse or accelerating breakup of the head vortex ring, both of which would reduce the penetration rate of the injection pulse.





$$w' = w - \bar{w}. \quad (17)$$

Figure 2. Vorticity contour (vorticity of 100,000) in a two-pulse jet at: (a) 0.25 ms, (b) 0.5 ms, (c) 0.75 ms, (d) 1.0 ms, and (e) 1.25 ms after start of injection of first pulse [5].

Figure 2 (a) shows the vorticity contours at 0.25 ms into the first pulse. The head-vortex is clearly evident. Figure 2 (b), 0.5 ms into the first pulse, shows the breakdown of the head vortex. At 0.5 ms, the first pulse ends. Figure 2 (c) shows the vorticity iso-surface at 0.75 ms, i.e. at the start of the second pulse. The region of turbulence from the first pulse is clearly evident in this figure. Figure 2(d) shows the contours at 1 ms, i.e. 0.25 ms into the second pulse. Comparing this figure with Fig. 2(a) which is 0.25 ms into the first pulse, it can be seen that the residual turbulence from the first pulse accelerates the breakdown of the head vortex of the second pulse. Figure 2 (e) shows the vorticity contours at the end of the second pulse.

Further insight can be gained by examining the centreline velocity plots in Fig. 3. Figure 3(a) shows the normalized centreline velocity 0.25 ms into the injection of the first pulse and 0.25 ms into the injection of the second pulse. It is evident by examining the results, that the second pulse is slightly accelerated by the first pulse. This is the bulk-velocity effect that we had referenced earlier. The region beyond an  $x/d$  of 10 shows the residual influence of the first pulse. Recall that at 0.25 ms after its injection, the second pulse is still fairly intact. Until this point, the effect appears to be a slight acceleration. Figure 3 (b) shows the centreline velocity 0.35 ms into the injection events of both pulses. The behaviour is now different in that the second pulse appears to have penetrated less, i.e. the acceleration effect is no longer evident. Between 0.25 and 0.35 ms, the head vortex of the second pulse has disintegrated faster as a result of the interaction with the first pulse and its penetration rate is decreased and mixing rate increased. This point is further emphasized in Fig. 4 which shows the axial velocity contours in the centre  $X$ - $Z$  plane of the jet at (a) 0.5 ms, i.e. at the end of the first pulse, and (b) 1.25 ms, i.e. at the end of the second pulse. It can be seen by examining the contours that the second pulse penetrates somewhat less and spreads more radially relative to the first pulse. Similar conclusions are arrived at by examining the radial velocity contours. As part of this study, different dwell times have been considered and it has been shown, not surprisingly, that shorter dwell times can accentuate the effects and longer dwell times attenuate them. The conclusion that the second head vortex is weaker and breaks up faster is consistent with the findings of Chikahia et al. [11].

The turbulent kinetic energy distribution was also examined. The turbulent kinetic energy  $k$  in the LES is calculated from the fluctuating velocity field as

$$k = 0.5(u'^2 + v'^2 + w'^2), \quad (14)$$

where each of the fluctuating velocity components  $u'$ ,  $v'$ , and  $w'$ , are

$$u' = u - \bar{u}, \quad (15)$$

$$v' = v - \bar{v}, \quad (16)$$

and

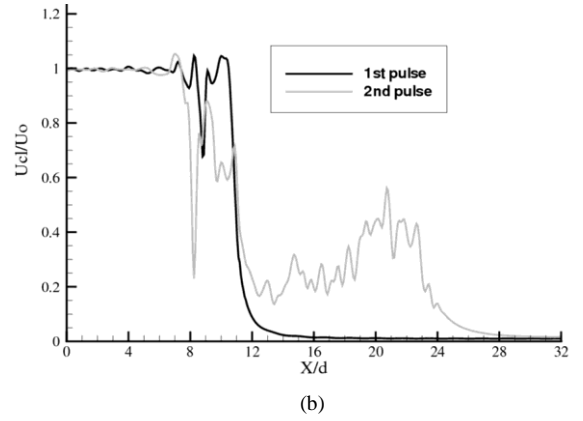
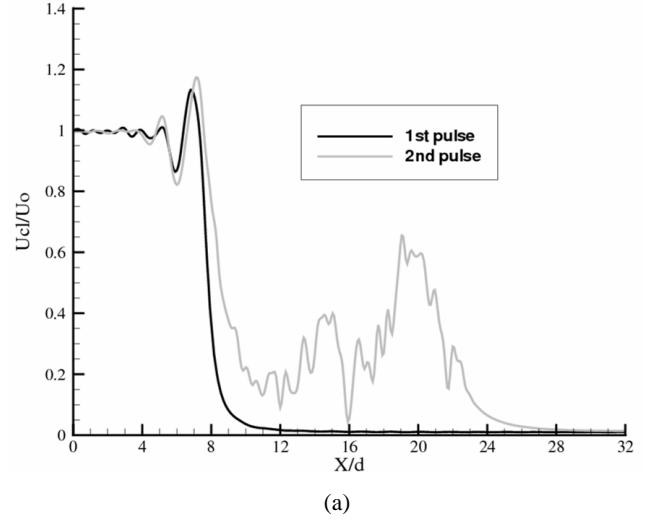


Figure 3. Centerline velocity for the two pulses (a) 0.25 ms after start of each pulse, and (b) 0.35 ms after start of each pulse [5].

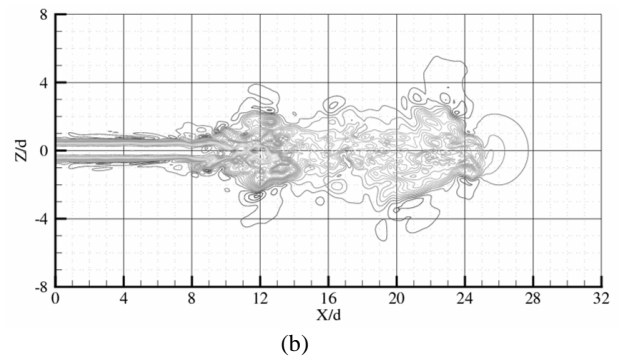
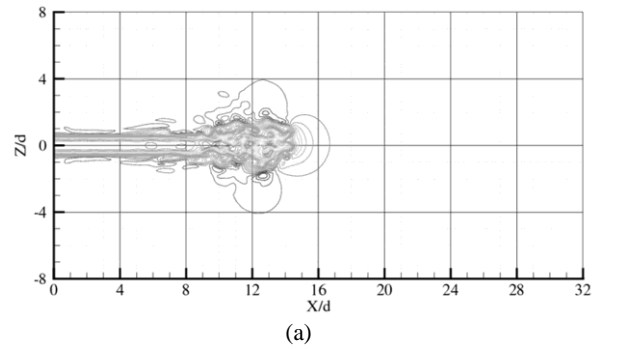


Figure 4. Axial velocity contours in a  $X$ - $Z$  plane intersecting the axis of the jet at (a) 0.5 ms, and (b) 1.25 ms [5].

Figure 5 shows the results. The upper half of the figure shows the turbulent kinetic energy contours 0.25 ms, i.e. midway into the first pulse, and the lower half shows the results at 1.0 ms, i.e. mid-way into the second pulse. It is interesting to note that although the second pulse disintegrates faster, the peak turbulent kinetic energy is about 14% lower than that in the first pulse. This reduction likely arises because of faster diffusion and dissipation that arises from the presence of the residual turbulence of the first pulse. It can also arise from the influence of the residual mean bulk velocity of the first pulse which can reduce the maximum velocity gradients. Additional details, including comparisons with Reynolds-Averaged Navier Stokes (RANS) simulation results and a critical discussion of the two sets of results may be found in Ref. [5].

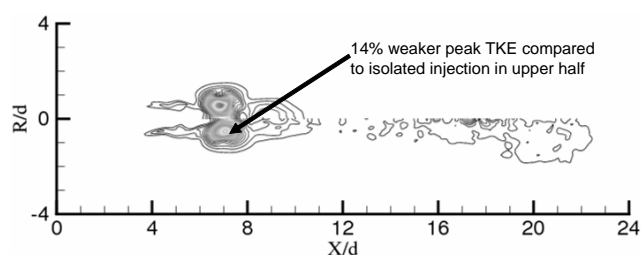


Figure 5. Mid-pulse comparison of turbulent kinetic energy. Top half shows results at 0.25 ms and the bottom half shows results at 1 ms [3].

## Conclusions

This study shows that in a two-pulse injection event, the head vortex of the jet resulting from the second injection initially penetrates faster, but the head vortex then disintegrates faster than the head vortex of the first pulse as a result of interaction with the residual turbulence from the first pulse. It is possible that there is a balance between the effect of the second pulse to penetrate farther, which can reduce mixing, and the effect of the residual turbulence to disintegrate the second pulse which can accelerate mixing. This balance may be influenced by dwell times. For the specific case considered here, the faster disintegration of the second pulse results in slower penetration and greater radial spreading of the second pulse.

## References

- [1] Abraham, J. & Pickett, L.M., Computed and Measured Fuel Vapor Distribution in a Diesel Spray, *Atomization and Sprays*, **20**, 2010, 241-250.
- [2] Bajaj, C., Abraham, J. & Pickett, L.M., Vaporization Effects on Transient Diesel Spray Structure, *Atomization and Sprays*, **21**, 2011, 411-426.
- [3] Abraham, J. & Magi, V., Exploring Velocity and Density Ratio Effects in a Mixing Layer Using DNS, Short Communication, *International Journal of Computational Fluid Dynamics*, **8**, 1997, 147-151.
- [4] Anders, J.W., Magi, V. & Abraham, J., Large-eddy Simulations in the Near Field of a Transient Multicomponent Gas Jet with Density Gradients, *Computers and Fluids*, **36**, 2007, 1609-1620.
- [5] Anders, J.W., Magi, V. & Abraham, J., A Computational Investigation of the Interaction of Pulses in Two-Pulse Jets, *Numerical Heat Transfer, Part A: Applications*, **54**, 2008, 999-1021.
- [6] Bogey, C., Bailly, C. & Juve, D., Noise Investigation of a High Subsonic Moderate Reynolds Number Jet Using a Compressible Large Eddy Simulation, *Theoretical Computational Fluid Dynamics*, **16**, 2003, 273-297.
- [7] Boree, J., Atassi, N. & Charnay, G., Phase Averaged Velocity Field in an Axisymmetric Jet Subject to a Sudden Velocity Decrease, *Experiments in Fluids*, **21**, 1996, 447-456.
- [8] Boree, J., Atassi, N., Charnay, G. & Taubert, L., Measurements and Image Analysis of the Turbulent Field in an Axisymmetric Jet Subject to a Sudden Velocity Decrease, *Experimental Thermal and Fluid Science*, **14**, 1997, 45-51.
- [9] Bremhorst, K. & Hollis, P.G., Velocity Field of an Axisymmetric Pulsed, Subsonic Air Jet, *AIAA Journal*, **28**, 1990, 2043-2049.
- [10] Carnahan, B., *Applied Numerical Methods*, p. 363, John Wiley & Sons, Inc., New York, 1969.
- [11] Chikahisa, T., Kaneko, T., Kikuta, K. & Hisanuma, Y., Significant NOx Formation at the Tip of Diesel Spray Flames and Its Reduction by Enhanced Mixing in the Tip Region, *SAE technical paper*, 2003, 2003-01-1786.
- [12] Erlebacher, G., Hussaini, M.Y., Speziale, C.G. & Zang, T.A., Toward the Large-Eddy Simulation of Compressible Turbulent Flows, *Journal of Fluid Mechanics*, **238**, 1992, 155-185.
- [13] Eroglu, A. & Breidenthal, R.E., Structure, Penetration, and Mixing of Pulsed Jets in Crossflow, *AIAA Journal*, **39**, 2001, 417-423.
- [14] Gill, S., A Process for the Step-by-Step Integration of Differential Equations in an Automatic Computing Machine, *Proceedings of the Cambridge Philosophical Society*, **47**, 1951, 96-108.
- [15] Husted, H.L., Piock, W. & Ramsay, G., Fuel Efficiency Improvements from Lean, Stratified Combustion with a Solenoid Injector, *SAE technical Paper*, 2009, 2009-01-1485.
- [16] Lee, C.S., Reitz, R.D. & Park, S.W., Effect of Split Injection on the Macroscopic Development and Atomization Characteristics of a Diesel Spray Injected Through a Common-Rail System, *Atomization Sprays*, **16**, 2006, 543-562.
- [17] Lele, S.K., Compact Finite Difference Schemes with Spectral-like Resolution, *Journal of Computational Physics*, **103**, 1992, 16-42.
- [18] Poinot, T.J. & Lele, S.K., Boundary Conditions for Direct Simulations of Compressible Viscous Flows, *Journal of Computational Physics*, **101**, 1992, 104-129.
- [19] Thomas, L.H., *Elliptic Problems in Linear Difference Equations Over a Network*, Watson Scientific Computing Laboratory Report, Columbia University Press, New York, 1949.
- [20] Zhang, Q. & Johari, H., Effects of Acceleration on Turbulent Jets, *Physics of Fluids*, **8**, 1996, 2185-2195.